



HAL
open science

Analysis of a thermoviscoelastic model in large strain

Stéphane Méo, Adnane Boukamel, Olivier Débordes

► **To cite this version:**

Stéphane Méo, Adnane Boukamel, Olivier Débordes. Analysis of a thermoviscoelastic model in large strain. *Computers & Structures*, 2002, 80, pp.2085-2098. 10.1016/S0045-7949(02)00246-8. hal-01236414

HAL Id: hal-01236414

<https://univ-tours.hal.science/hal-01236414>

Submitted on 10 Feb 2018

HAL is a multi-disciplinary open access archive for the deposit and dissemination of scientific research documents, whether they are published or not. The documents may come from teaching and research institutions in France or abroad, or from public or private research centers.

L'archive ouverte pluridisciplinaire **HAL**, est destinée au dépôt et à la diffusion de documents scientifiques de niveau recherche, publiés ou non, émanant des établissements d'enseignement et de recherche français ou étrangers, des laboratoires publics ou privés.

Analysis of a thermoviscoelastic model in large strain

S. Méo^{a,*}, A. Boukamel^{a,b}, O. Débordes^a

^a *Laboratoire de Mécanique et d'Acoustique de Marseille, UPR CNRS 7051, IMT/ESM2, Technopole de Château Gombert, 13451 Marseille Cedex 20, France*

^b *Ecole Supérieure d'Ingénieurs de Marseille, Technopole de Château Gombert, 13451 Marseille Cedex 20, France*

This paper deals with a thermoviscoelastic model and its analysis. The mechanical formulation is based on the generalization to large strain of the Poynting–Thomson rheological model. The heat transfers are governed by the classical heat equation and the Fourier law. We briefly expose the finite element formulation, which takes into account the quasi-incompressibility constraint for the mechanical approach. The influence of several parameters is examined.

1. Introduction

Nowadays, elastomers are frequently employed in many sectors such as automobile and aeronautics industries. In their uses, these materials can undergo strong mechanical and thermal loadings. Moreover their mechanical properties highly depend on the temperature and thus the prediction of the behaviour and the assessment of the fatigue strength require a local analysis based on a formulation of thermomechanical models.

The behavior of an elastomer can be very different according to:

- the temperature,
- the degree of crosslinking,
- the incorporated particles (carbon black or silicium filled rubbers)
- ...

So we can distinguish several approaches in the literature in accordance with the considered phenomenon:

- hyperelasticity modeling the static behaviour of the material,
- continuum damage mechanics approaching the softening behaviour under deformation, currently call Mullins' effect [28],
- nonlinear viscoelasticity for the simulation of the relaxation phenomenon and the eventual dissipation,
- thermomechanical coupling to take temperature sensitivity of mechanical characteristics into account and to describe the temperature changes due to the mechanical dissipation.

More precisely, for hyperelasticity several stress strain relationships are proposed which are based on the expression of strain energy density in the isotropic, incompressible materials or very nearly so (almost incompressible). Among these behaviour laws, statistical models were carried out with entropic consideration of the molecular chains configurations [38,39], an other way consists in a phenomenological approach deduced from isotropy and incompressibility. These last ones must be adjusted according to experiment [12,26,31, 32].

Rubber materials, especially carbon black-filled, present a softening effect experimentally observed [13]. This loss of stiffness can be micro-mechanically described by a local separation of the carbon and rubber.

* Corresponding author. Fax: +33-4-91-05-44-58.
E-mail address: meo@imtumn.esm2.imt-mrs.fr (S. Meo).

- Coupling the aspects of statistical mechanics and composite material theory, Govindjee and Simo [10] propose a first model. It is based on the relation between the free energy for a statically representative sample volume and the polymer chains free energy (the particles are assumed to be rigid). This last energy is additively split into the contribution of the chains that are crosslinked on both ends and the contribution of the chains attached on both ends to carbon particles.

Some phenomenological considerations allow an efficient numerical implementation of this model [9].

- A complete phenomenological model is describe by Simo [37] for a viscoelastic material. It includes softening behavior under deformation for a cyclic test with increasing amplitude.

The last two models take only discontinuous damage into account because the damage is related to the maximum stretch of the deformation history for the first and to the maximum effective strain energy for the second. But, experimental investigations show that the filled polymers present a damage accumulation for all strain cycles and not only for increasing amplitude strain cycles. To take this into account, Miehe [25] uses a damage evolution governed by the arclength of the effective strain-energy.

Furthermore, concerning the nonlinear viscoelastic aspects the formulations are categorized as follows:

- the integral approach principally developed for nonlinear materials with fading memory and which give the stress tensor according to the strain history [4, 5,32].

The finite linear viscoelasticity method [6,21] is a direct application. It is based on a modified linear Boltzmann superposition principle with a nonlinear strain measure. It uses an asymptotic expansion of relaxation functions. The separability principle between strain and time is expressed by the first term of the expansion, while the higher order terms constitute a correction. More recently, a generalized deformation measure is proposed in a modified finite linear viscoelasticity theory [3,27].

- the differential approach is based on the concept of intermediate state commonly used to describe finite elastic–plastic deformations [33,34]. It can be saw as a generalization to large strains of classical rheological models [17,18,20,36]. The local state method [19] constitutes the theoretical frame of this formulation, the internal variables being introduced by the intermediate states.

These approaches are often more adapted to nuerical developments.

The inelastic material properties of elastomers involve an internal heat production and thus an increase of the temperature. This thermomechanical coupling phenomenon is studied by Holzapfel and Simo [15], but this paper is only concerned with the linear viscoelasticity. The theoretical framework of a fully coupled thermomechanical behaviour for finite strains is developed in the case of elasticity in [15] by the decomposition of transformation into a thermal one and an elastic one. The same idea is employed by Lion [22] but instead of an elastic part, the mechanical transformation is viscoelastic. The internal variables of this models correspond to inelastic deformations tensors. Holzapfel and Simo [16] realized the same description but using internal variables of stress type. All these studies give guidelines to handle nonisothermal problems, taking thermomechanical coupling into account.

Besides the mechanical (or thermomechanical) behaviour, on the numerical aspects, many works contribute to the development of mathematical formulation and numerical methods allowing precise simulations of hyperelastic or viscoelastic materials. These finite element formulations allow the large strains and take the incompressibility constraint into account using a penalty method [23,29] or an augmented Lagrangian method [8] in order to solve the equilibrium problem in hyperelasticity. Le Tallec and Rahier [18] use a similar approach for the nonlinear viscoelasticity with a local treatment of internal variables.

In this paper, we present a thermoviscoelastic model for large deformation and finite variations of temperature. It is based on a fully phenomenological approach, on irreversible thermodynamics and on the local state method.

After a presentation of the mechanical, thermal and coupling aspects, we will give an influence analysis of different parameters taking into account in these aspects.

2. Model presentation

2.1. Kinematical description

Consider a body occupying the domain Ω in the undeformed C_0 and ω in the current configuration C_t (Fig. 1).

As usual, $\overline{\overline{C}}$ defines the right Cauchy–Green tensor, $\overline{\overline{E}}$ the Euler–Almansi strain tensor, $\overline{\overline{L}}$ the velocity gradient and $\overline{\overline{D}}$ the rate of deformation. They can be defined from $\overline{\overline{F}}$ the deformation gradient:

$$\overline{\overline{C}} = \overline{\overline{F}}^T \cdot \overline{\overline{F}}, \quad (1)$$

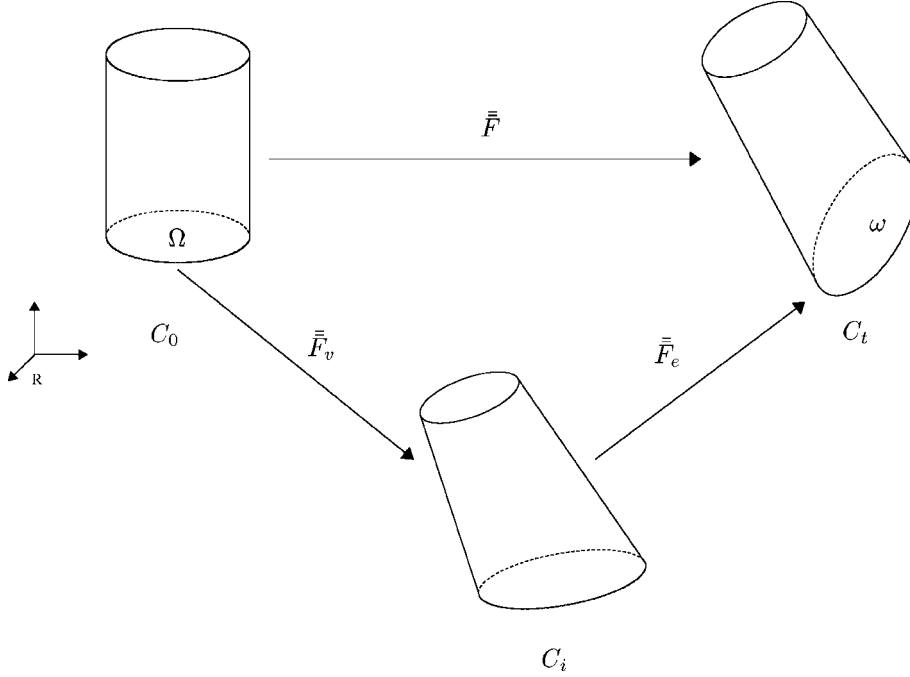


Fig. 1. System configurations.

$$\bar{\bar{E}} = \frac{1}{2}(\bar{\bar{C}} - \bar{\bar{I}}), \quad (2)$$

$$\bar{\bar{L}} = \dot{\bar{\bar{F}}} \cdot \bar{\bar{F}}^{-1}, \quad (3)$$

$$\bar{\bar{D}} = \frac{1}{2}(\bar{\bar{L}} + \bar{\bar{L}}^T). \quad (4)$$

The additive decomposition of infinitesimal strain tensor ($\bar{\bar{e}}$) into an elastic part ($\bar{\bar{e}}_e$) and an inelastic one ($\bar{\bar{e}}_a$):

$$\bar{\bar{e}} = \bar{\bar{e}}_e + \bar{\bar{e}}_a \quad (5)$$

can be extended to large deformation by means of the intermediate state C_i (Fig. 1) [35]. Introducing $\bar{\bar{F}}_e$ and $\bar{\bar{F}}_v$ respectively, the pseudo-gradients of elastic and viscous motion, the deformation gradient can be decomposed as:

$$\bar{\bar{F}} = \bar{\bar{F}}_e \cdot \bar{\bar{F}}_v. \quad (6)$$

It is possible to define an elastic and a viscous dilatation tensor:

$$\bar{\bar{C}}_v = \bar{\bar{F}}_v^T \cdot \bar{\bar{F}}_v, \quad (7)$$

$$\bar{\bar{C}}_e = \bar{\bar{F}}_e^T \cdot \bar{\bar{F}}_e. \quad (8)$$

2.2. Thermodynamic formulation

The system transformation is governed by three conservation laws of the classical thermodynamics, locally written in Lagrangian description.

- Mass conservation:

$$\rho_0(\det \bar{\bar{F}}) = \rho_0, \quad (9)$$

- Momentum conservation:

$$\rho_0 \dot{\bar{\bar{u}}} = \text{div}_X \bar{\bar{\pi}} + \rho_0 \bar{\bar{f}}, \quad (10)$$

- Energy conservation:

$$\rho_0 \dot{e} = \bar{\bar{\pi}} : \dot{\bar{\bar{F}}} - \text{div}_X \bar{\bar{Q}} + \rho_0 r \quad (11)$$

with ρ_0 and ρ respectively the local density mass in C_0 and C_t , $\bar{\bar{\pi}}$ the first Piola–Kirschhoff stress tensor, $\bar{\bar{f}}$ the specific forces, e the specific internal energy, $\bar{\bar{Q}}$ the Piola–Kirschhoff heat flux and r the rate of heat production per unit mass. According to the theory of the thermodynamics of irreversible processes (local state method [19]), an independent set of thermodynamics variables is chosen (see [7]): $(\bar{\bar{C}}, \bar{\bar{C}}_v, T)$, where T is the absolute temperature.

Introducing ψ , the specific free energy, as a function of this variables set and (11) in the Lagrangian description of the Clausius–Duhem inequality:

$$\phi_0 = \underbrace{\left(\pi - \frac{\partial \psi}{\partial \bar{F}} \right) : \dot{\bar{F}} - \rho_0 \left(\eta + \frac{\partial \psi}{\partial T} \right) \dot{T} - \rho_0 \frac{\partial \psi}{\partial \bar{C}_v} : \dot{\bar{C}}_v}_{\phi^{\text{int}}} - \underbrace{\frac{1}{T} \dot{\bar{Q}} \cdot \text{grad}_x T}_{\phi^{\text{the}}} \geq 0. \quad (12)$$

We suppose the mechanical (often called intrinsic) and thermal effects uncoupled in (12):

$$\phi^{\text{int}} \geq 0 \quad \text{and} \quad \phi^{\text{the}} \geq 0. \quad (13)$$

Under the assumption of normal dissipation only depending on the internal variables (the material presents an instantaneous elasticity) and T , the behaviour law and the evolution equations of \bar{C}_v and T [11] are obtained:

$$\begin{cases} \bar{\pi} = \rho_0 \frac{\partial}{\partial \bar{F}} \psi(\bar{C}, \bar{C}_v, T), \\ \eta = \frac{\partial \psi}{\partial T}, \\ -\rho_0 \frac{\partial}{\partial \bar{C}_v} \psi(\bar{C}, \bar{C}_v, T) = \frac{\partial}{\partial \bar{C}_v} \phi^{\text{int}}(\bar{C}_v), \\ -\frac{\text{grad}_x T}{T} = \frac{\partial}{\partial \bar{q}} \phi^{\text{the}}(\bar{q}). \end{cases} \quad (14)$$

This yields for intrinsic dissipation:

$$\phi^{\text{int}} = v \frac{\partial \phi}{\partial \dot{\bar{C}}_v}. \quad (15)$$

Remark 1. The high compressibility modulus of the considered elastomer and the range of the evolution of the temperature (see Section 5.4) make that the dilations induced by heating effect are very small and are thus negligible. Consequently, our model does not include thermal dissipation effect.

2.3. Mechanical behaviour

The mechanical constitutive equations are obtain by the generalization to large strain of the rheological model of Poynting–Thomson (Fig. 2). To argue from

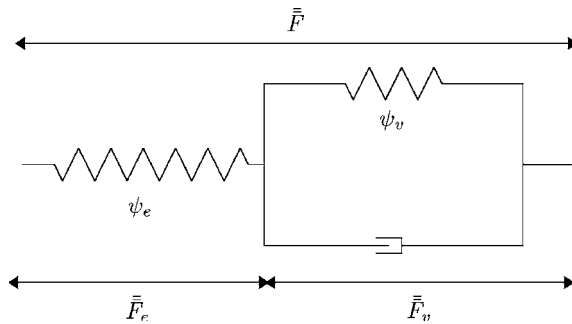


Fig. 2. Poynting–Thomson model.

analogy with small perturbations, the total free energy is split into two parts ψ_e and ψ_v . They are defined as the free specific energies associated respectively to elasticity and viscous responses of the material. For both these two quantities, we choose an incompressible hyperelastic law of Gent–Thomas for instantaneous elasticity (ψ_e) and a Neoohooke one for ψ_v :

$$\begin{cases} \psi_e = c_1(T)(I_1 - 3) + c_2(T) \ln \frac{I_1}{3}, \\ \psi_v = a_1(T)(I_1 - 3). \end{cases} \quad (16)$$

The three material coefficients c_1 , c_2 , a_1 are experimentally determined and they are considered temperature dependent.

The incompressibility constraint is applied to \bar{C} and \bar{C}_v

$$\det \bar{C} = 1, \quad \text{tr}(\dot{\bar{C}}_v \cdot \bar{C}_v^{-1}) = 0. \quad (17)$$

The total free energy is then given by:

$$\rho_0 \psi(\bar{C}, \bar{C}_v, T) = \begin{cases} \rho_0 (\psi_e(\bar{C}, T) + \psi_v(\bar{C}_v, T)) & \text{if } \det \bar{C} = 1, \\ \infty & \text{otherwise.} \end{cases} \quad (18)$$

The dissipation is assumed to only depend on the internal variable. The mechanical pseudo-potential of dissipation ϕ is taken as a quadratic function of $\dot{\bar{C}}_v$:

$$\phi(\dot{\bar{C}}_v, T) = \begin{cases} \frac{1}{2} v(T) \dot{\bar{C}}_v : \dot{\bar{C}}_v & \text{if } \text{tr}(\dot{\bar{C}}_v \cdot \bar{C}_v^{-1}) = 0, \\ \infty & \text{otherwise} \end{cases} \quad (19)$$

with v a fourth material coefficient temperature dependent. The evolution of v , c_1 , c_2 , a_1 are determined at the same time (see Sections 4 and 5.1).

We then substitute (18) and (19) in (14) for the Poynting–Thomson rheological model:

$$\begin{cases} \pi = 2\rho_0 \bar{F}_e \cdot \left[\left(\frac{\partial \psi_e}{\partial I_1^e} + \frac{\partial \psi_e}{\partial I_2^e} I_1^e \right) \bar{1} - \frac{\partial \psi_e}{\partial I_2^e} \bar{C}_e \right] \cdot \bar{F}_v^{-T} + p \text{cof } \bar{F}, \\ -\rho_0 \bar{C}_v^{-1} \cdot \bar{C} \cdot \left[\left(\frac{\partial \psi_e}{\partial I_1^e} + \frac{\partial \psi_e}{\partial I_2^e} I_1^e \right) \bar{1} - \frac{\partial \psi_e}{\partial I_2^e} \bar{C}_v^{-1} \cdot \bar{C} \right] \cdot \bar{C}_v^{-1} \\ + \rho_0 \frac{\partial \psi_v}{\partial I_1^v} \bar{1} + v \dot{\bar{C}}_v + q \bar{C}_v^{-1} = 0, \\ \det \bar{C} = 1, \\ \text{tr}(\dot{\bar{C}}_v \cdot \bar{C}_v^{-1}) = 0. \end{cases} \quad (20)$$

where p and q are Lagrange multipliers which impose the incompressibility constraints (20c and d). Then

multiplying (20b) by $\bar{\bar{C}}_v$ and only considering its deviatoric part, q is eliminated and we obtain:

$$\begin{cases} \rho_0 \left[\bar{\bar{C}} \cdot \left(\left(\frac{\partial \psi_e}{\partial I_1^e} + \frac{\partial \psi_e}{\partial I_2^e} I_1^e \right) \bar{\bar{I}} - \frac{\partial \psi_e}{\partial I_2^e} \bar{\bar{C}}_v^{-1} \cdot \bar{\bar{C}} \right) \cdot \bar{\bar{C}}_v^{-1} \right]^D \\ + \rho_0 \frac{\partial \psi_v}{\partial I_1^v} \bar{\bar{C}}_v^D + v [\bar{\bar{C}}_v \cdot \dot{\bar{\bar{C}}}_v]^D = 0, \\ \text{tr}(\dot{\bar{\bar{C}}}_v \cdot \bar{\bar{C}}_v^{-1}) = 0. \end{cases} \quad (21)$$

2.4. Thermal behaviour

The Piola–Kirschhoff heat flux (\vec{Q}) is given by the Fourier law written in the current configuration:

$$\vec{Q} = -\bar{\bar{K}}_L \cdot \nabla_{\vec{X}} T(\vec{X}, T). \quad (22)$$

In this relation, the conductivity tensor ($\bar{\bar{K}}_L$) is expressed in the initial configuration by:

$$\bar{\bar{K}}_L = \bar{\bar{F}}^{-1} \cdot \bar{\bar{K}} \cdot \bar{\bar{F}}^{-T}, \quad (23)$$

$\bar{\bar{K}}$ being the usual Eulerian conductivity tensor.

3. Coupling model

3.1. Constitutive equations

3.1.1. Mechanical problem

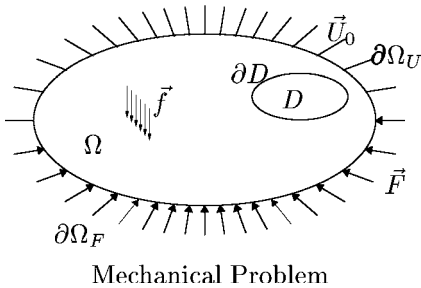
The governing equations of the mechanical problem are given by the mass and momentum conservation laws, under the hypothesis of incompressibility medium:

$$\frac{\rho}{\rho_0} = \det \bar{\bar{F}} = 1 \quad \forall \vec{X} \in \Omega, \quad (24)$$

$$\rho_0 \ddot{\vec{u}} = \text{div} \bar{\bar{\pi}} + \rho_0 \vec{f} \quad \forall \vec{X} \in \Omega \quad (25)$$

with the boundary conditions (see Fig. 3(a)):

$$\begin{cases} \bar{\bar{\pi}} \cdot \vec{N} = \vec{F} & \forall \vec{X} \in \partial\Omega_F, \\ \vec{u} = \vec{U}_0 & \forall \vec{X} \in \partial\Omega_U, \\ \partial\Omega_F \cap \partial\Omega_U = \emptyset & \partial\Omega_F \cup \partial\Omega_U = \partial\Omega. \end{cases} \quad (26)$$



It is pointed out that $\bar{\bar{\pi}}$ depends on the temperature through the coefficients c_1 , c_2 , a_1 and v (see Section 2.3).

3.1.2. Thermal problem

The heat transfers are governed by the classical heat equation written in Lagrangian description [1]:

$$\rho_0 C_e \dot{T} = -\text{div} \vec{Q} + \rho_0 r + D_s, \quad (27)$$

where C_e is the heat capacity:

$$C_e = T \frac{\partial s}{\partial T}, \quad (28)$$

$\rho_0 r$ the classical internal source term and

$$D_s = \underbrace{v \dot{\bar{\bar{C}}}_v : \dot{\bar{\bar{C}}}_v}_{\textcircled{1}} + \rho_0 T \underbrace{\left(\frac{\partial^2 \psi}{\partial T \partial \bar{\bar{C}}} : \dot{\bar{\bar{C}}} + \frac{\partial^2 \psi}{\partial T \partial \bar{\bar{C}}_v} : \dot{\bar{\bar{C}}}_v \right)}_{\textcircled{2}} \quad (29)$$

is the internal source term per volume unit in the initial configuration due to the mechanical problems. It can be split into two parts, $\textcircled{1}$ is the intrinsic mechanical dissipation and $\textcircled{2}$ represents the dependence between the thermal problem and mechanical one.

Remark 2. We will see later that the mechanical and the thermal problems will be solved sequentially. During one mechanical step (< 1 s), the evolution of the temperature remains imperceptible. So we can consider that the term $\textcircled{2}$ can be neglected $\partial \psi / \partial T \rightarrow 0$. Thus the source term is reduced to the intrinsic dissipation.

The boundary conditions are given by (see Fig. 3(b))

$$\begin{cases} \vec{Q} = \vec{Q}_s & \forall \vec{X} \in \partial\Omega_Q, \\ T = \theta & \forall \vec{X} \in \partial\Omega_T, \\ \partial\Omega_Q \cap \partial\Omega_T = \emptyset & \partial\Omega_Q \cup \partial\Omega_T = \partial\Omega. \end{cases} \quad (30)$$

3.2. Variational formulations

For the mechanical problem the variational formulation of the quasi-static equilibrium problem is obtain

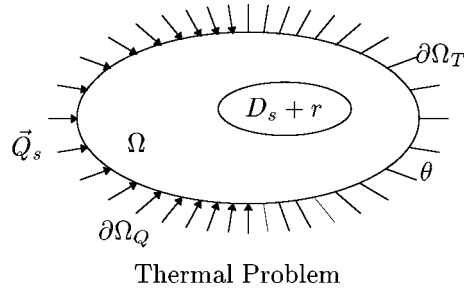


Fig. 3. Thermomechanical problem and boundary conditions.

by a perturbed Lagrangian form.¹ The solution $(\bar{\mathbf{u}}, p)$ has to cancel the following integral form for all the test functions $\delta\bar{\mathbf{u}}$ and δp chosen respectively in the same spaces as those of the trial functions $\bar{\mathbf{u}}$ and p :

$$\begin{aligned} \mathfrak{I}^{\text{mec}}(\bar{\mathbf{u}}, p) = & \int_{\Omega} \bar{\pi} : \delta\bar{\mathbf{F}} dV - \int_{\partial\Omega_f} \bar{\mathbf{F}} \cdot \delta\bar{\mathbf{u}} dS \\ & - \int_{\Omega} \rho_0 \bar{\mathbf{f}} \cdot \delta\bar{\mathbf{u}} dV + \int_{\Omega} \delta p (J - 1 - \alpha p) dV, \end{aligned} \quad (31)$$

α is a perturbation term, which is equal to zero when the solution satisfies the incompressibility constraints (20c and d). If it is strictly positive but small, the obtained solution satisfies the quasi-incompressibility condition. For our problem, we take $\alpha = 5 \times 10^{-4} \text{ MPa}^{-1}$.

The solution of the thermal problem has to cancel for all test functions δT :

$$\begin{aligned} \mathfrak{I}^{\text{the}}(T) = & - \int_{\partial\Omega_Q} \bar{\mathbf{Q}} \cdot \bar{\mathbf{N}} \delta T dS - \int_{\Omega} (D_s + \rho_0 r) \delta T dV \\ & + \int_{\Omega} (\rho_0 C_p \bar{\mathbf{T}} \delta T + \bar{\nabla}_L(\delta T) \cdot \bar{\mathbf{K}}_L \cdot \bar{\nabla}_L(T)) dV. \end{aligned} \quad (32)$$

3.3. Finite element approximation

3.3.1. Mechanical problem

We choose for the mechanical problem a classical two-dimensional triangular finite element with a quadratic interpolation for the displacement and a constant pressure. It is commonly called T6/P1. It verifies the discrete LBB condition and yields stable pressure approximations [30]. The hydrostatic pressure is assumed as an internal degree of freedom, which is eliminated by a static condensation at element level.

When we use an isoparametric interpolation the displacement is given by:

$$\bar{\mathbf{u}} = [N_u^e] \{U^e\}, \quad (33)$$

$$\{\bar{\mathbf{F}}\} = [B^e] \{U^e\} + \{\bar{\mathbf{I}}\}, \quad (34)$$

and the constant pressure is given by:

$$p = \langle N_p^e \rangle \{P^e\}. \quad (35)$$

Eqs. (33)–(35) allow the discretization of (31). Then its resolution requires the implementation of an iterative algorithm of Newton–Raphson giving, at each iteration, the linear system:

$$\begin{cases} \sum_{e=1}^{\text{Nelt}} \langle \delta U^e \rangle ([k_t^e] \{\Delta U^e\} + [g^e] \{\Delta P^e\} + \{r^e\}) = 0, \\ \sum_{e=1}^{\text{Nelt}} \langle \delta g^e \rangle ([g^e]^T \{\Delta U^e\} + [a^e] \{\Delta P^e\} + \{i^e\}) = 0 \end{cases} \quad (36)$$

with the elementary vectors and matrix given by:

- the tangent matrix:

$$[k_t^e] = \int_{v^e} [B^e]^T \left[\frac{\partial \bar{\pi}}{\partial \{u^e\}} \right] dv, \quad (37)$$

- the residue vector:

$$\begin{aligned} \{r^e\} = & \int_{v^e} [B^e]^T \{\bar{\pi}\} dv - \int_{v^e} [N_u^e]^T \{\bar{\mathbf{f}}\} dv \\ & - \int_{v^e \cap \partial\Omega_f} [N_u^e]^T \{\bar{\mathbf{F}}\} ds, \end{aligned} \quad (38)$$

- the incompressibility matrix:

$$[g^e] = \int_{v^e} [B^e]^T \{\text{cof } \bar{\mathbf{F}}\} \langle N_p^e \rangle dv, \quad (39)$$

- the perturbation matrix:

$$[a_p^e] = \alpha \int_{v^e} \{N_p^e\} \langle N_p^e \rangle dv, \quad (40)$$

- and the incompressibility residue:

$$\{i^e\} = \int_{v^e} \{N_p^e\} (J - 1 - \alpha p) dv^e. \quad (41)$$

After the static condensation, the iterative global system is finally obtained:

$$[K_{ic}] \{\Delta u\} = \{R_c\} \quad (42)$$

with

$$\begin{cases} [K_{ic}] = A_{e=1}^{\text{Nelt}} ([k_t^e] + [g^e] [a_p^e] [g^e]^T), \\ \{R_c\} = A_{e=1}^{\text{Nelt}} (-\{r^e\} + [g^e] [a_p^e]^{-1} \{i^e\}), \end{cases} \quad (43)$$

where $A_{e=1}^{\text{Nelt}}$ represents the classical assembly operator of the finite elements method.²

3.3.2. Thermal problem

For the thermal problem, we use the same geometric discretization, but using a linear interpolation for temperature:

$$T = \langle N_\theta^e \rangle \{T^e\}. \quad (44)$$

Using (44), the integral form (32) leads to:

$$[M_\theta] \{\dot{T}\} + [K_\theta] \{T\} = \{F_\theta\} \quad (45)$$

¹ This method is equivalent to a method of penalization with a reduced and selective integration technique [2,24].

² This operator allows to pass from vectors or matrix $([k_t^e], \{r^e\}, \dots)$ to the global matrix $[K_{ic}]$ and to the global vector $\{R_c\}$.

with the mass matrix, the stiffness matrix and the body forces given by:

$$[M_\theta] = \frac{A}{e=1} \int_{v^e} \rho_0 C_p \{N_\theta^e\} \langle N_\theta^e \rangle dv, \quad (46)$$

$$[K_\theta] = \frac{A}{e=1} \int_{v^e} [B^e]^T [K_L] [B^e] dv, \quad (47)$$

$$\{F_\theta\} = \frac{A}{e=1} \int_{v^e} \{N_\theta^e\} (D_s + \rho_0 r) dv + \int_{v^e \cap \partial\Omega_Q} \{N_\theta^e\} \vec{Q} \cdot \vec{N} ds. \quad (48)$$

Then the differential system (45) is solved by an implicit Eulerian time integration scheme.

3.4. Local solving of complementary law

The construction of the mechanical elementary matrices and vectors requires the evaluation, at each integration point, of the internal variable $\bar{\bar{C}}_v$ and the derivative term $\partial\bar{\bar{C}}_v/\partial\bar{\bar{F}}$. The complementary law (21) is summarized by:

$$\begin{cases} \dot{\bar{\bar{C}}}_v = \bar{\bar{\chi}}(t, \bar{\bar{F}}(t), \bar{\bar{C}}_v(t)) & \text{on } [t_0, t_0 + \Delta t], \\ \bar{\bar{C}}_v(t_0) = \bar{\bar{C}}_v^0. \end{cases} \quad (49)$$

By means of an implicit Eulerian scheme, (49) gives on $[t_n, t_n + \delta t]$ a sub-interval of $[t_0, t_0 + \Delta t]$:

$$\bar{\bar{C}}_v(t_{n+1}) = \bar{\bar{C}}_v(t_n) + \delta t \bar{\bar{\chi}}(t_{n+1}, \bar{\bar{F}}(t_{n+1}), \bar{\bar{C}}_v(t_{n+1})) \quad (50)$$

which is solved by a Newton–Raphson scheme.

The term $\partial\bar{\bar{C}}_v/\partial\bar{\bar{F}}$ is given by the linear system:

$$\begin{cases} \frac{d\bar{\bar{C}}_v}{d\bar{\bar{F}}} = \frac{\partial\bar{\bar{\chi}}}{\partial\bar{\bar{C}}_v} : \frac{\partial\bar{\bar{C}}_v}{\partial\bar{\bar{F}}} + \frac{\partial\bar{\bar{\chi}}}{\partial\bar{\bar{F}}} & \text{on } [t_0, t_0 + \Delta t], \\ \left. \frac{\partial\bar{\bar{C}}_v}{\partial\bar{\bar{F}}} \right|_{t=t_0} = 0. \end{cases} \quad (51)$$

Using the approximate solution of (51) (and thus the same time step) (51) can be solved by a Crank–Nicholson scheme.

3.5. Coupling algorithm

The time scale of the mechanical problem is assumed to be smaller than the thermal one in this algorithm. Thus these problems can be solved separately. Considering an evolution of the mechanical parameters experimentally determined, the algorithm described Fig. 4 is adopted.

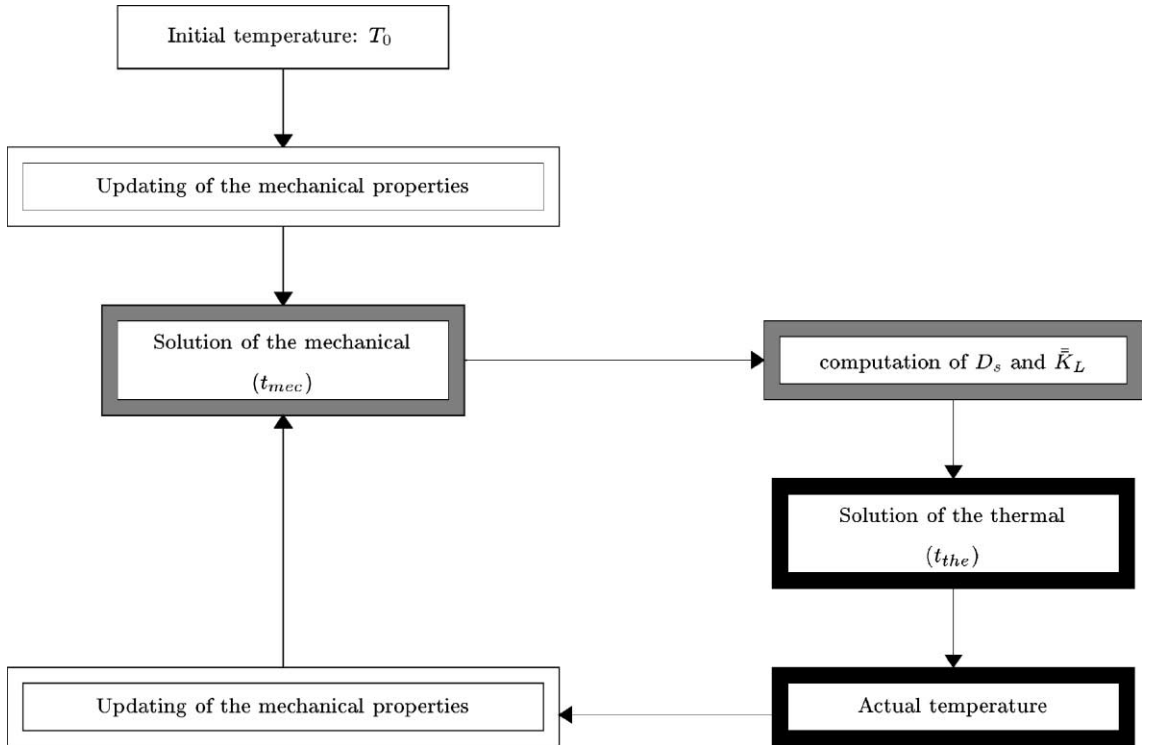


Fig. 4. Coupling algorithm.

We first start from a mechanical computation, after stabilization, a mechanical term source (the mechanical dissipation or its average, see Section 5.2) and eventually the gradient transformation are transmitted to the thermal model. We can now run a thermal simulation, once the evolution of the temperature is sufficient, the mechanical properties are updated, a new mechanical computation is started, and so on.

An appropriate choice of t_{mec} and t_{the} (Fig. 4) could lead to the same time scales for the mechanical and thermal computations.

4. Identification of the mechanical characteristics

The identification procedure consists in a least square fitting. Cyclic loadings (broken line, Fig. 5(b)) are used. These experimental data are decomposed in two: the average stress of a stabilized cycle (broken line, Fig. 5(a)) and the stress difference at constant strain during the rise and fall of the hysteresis curve (broken line, Fig. 5(c)).

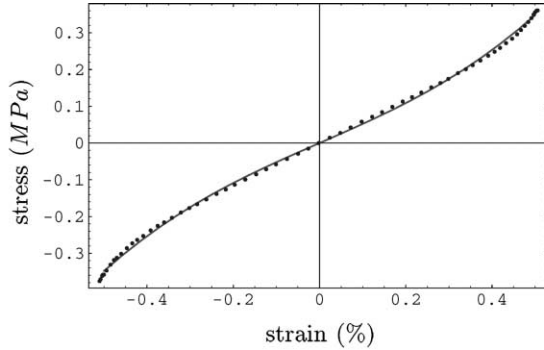
Identifying the average curve to a shearing hyper-elastic curve (Gent–Thomas model) (continuous line, Fig. 5(a)), a first value (C_1, C_2) is determined. Then from this result, a correction and a complete determination is provided according to an heuristic method (continuous line, Fig. 5(b)–(d)) and a set of variables (C_1, C_2, A_1, v) is finally obtained.

5. Numerical simulation

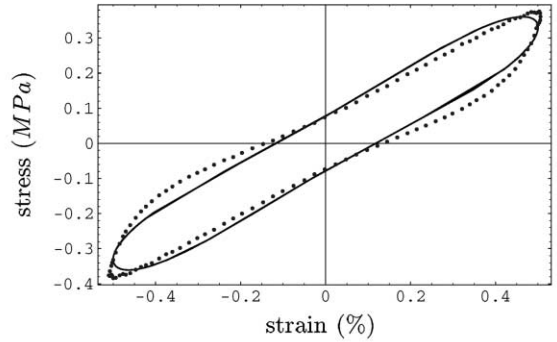
The different tests are realized on a two-layer elastomer-steel test piece (Fig. 6(a)). The elastomer part is made dimethyl-vinyl-siloxan vulcanized by peroxide.

This test piece is put into a thermal enclosure at a constant temperature and subjected to a cyclic shearing deformation, $\gamma(t) = \Gamma \sin(2\pi ft)$, with a frequency f of 3.1 Hz. The amplitude Γ defines the relative shearing displacement applied to the external armatures while the central armature is clamped.

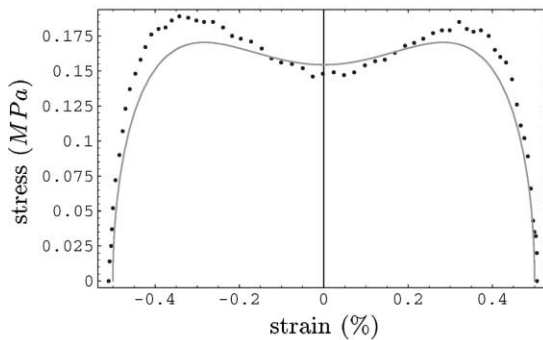
Two thermocouples measure the temperature on one of the elastomeric layers (Fig. 6(a)).



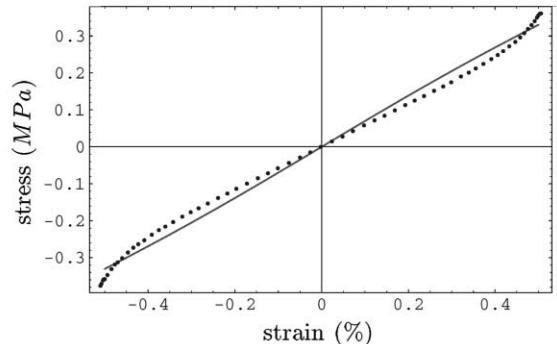
(a) Experimental average stress and numerical identification of Gent-Thomas model.



(b) Experimental and numerical hysteresis.



(c) Experimental and numerical stress difference.



(d) Experimental and numerical average stress.

Fig. 5. Experimental (\dots) and identified ($—$) curves.

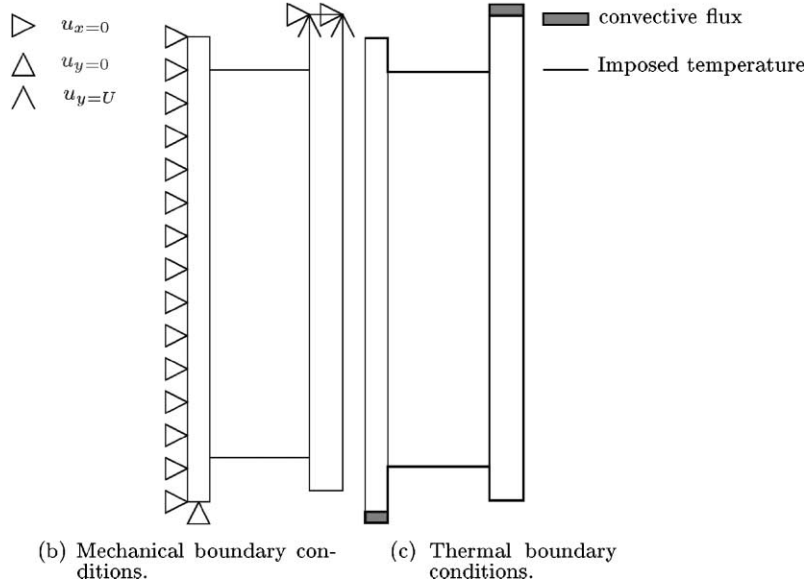
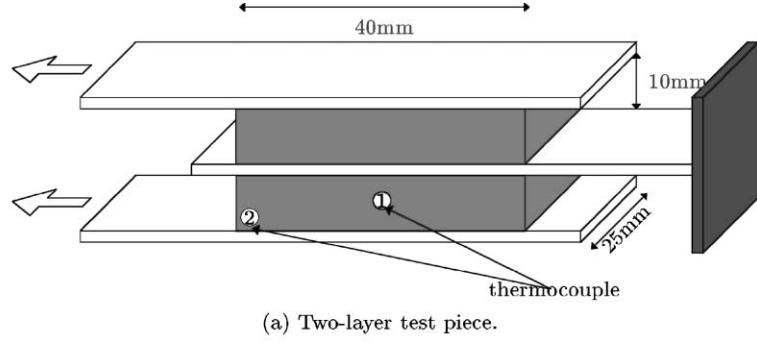


Fig. 6. Physical and numerical problems.

5.1. Modelisation

Due to the symmetry of the problem, the computation of this shearing test has been carried out on a half cross-section of the test piece.

For the thermal problem (Fig. 6(c)), linear triangular, linear quadrilateral and linear flux elements are used to mesh respectively the elastomeric layer, the metallic armatures and the boundaries. A zero flux condition is applied on the symmetry axis and a convective heat transfer condition is imposed on other boundaries:

$$\vec{Q} = -h(T - T_0)\vec{N},$$

where h is convective heat coefficient and T_0 the temperature of the thermal enclosure. The values of the thermal properties of the materials are declined Table 1.

For the mechanical problem (Fig. 6(b)), using the plane strains hypothesis, the mesh is the same as the

Table 1
Thermal properties

	Elastomer	Steel
K ($\text{W m}^{-1} \text{K}^{-1}$)	0.127	45
$\rho_0 C_e$ ($\text{J m}^{-3} \text{K}^{-1}$)	0.74×10^6	3.5×10^6
h ($\text{W m}^{-2} \text{K}^{-1}$)	17	30

thermal one (without the linear flux elements), but a quadratic interpolation is used. The boundary conditions are:

- no displacement on the fixed edge of the central armature,
- a sinusoidal displacement on the loaded edges of outer armatures.

Moreover, on the symmetry axis, the normal displacement is fixed to zero. The mechanical properties of

Table 2
Mechanical properties of steel

Young modulus E (MPa)	210000
Poisson ratio ν	0.3

the materials are given Table 2. For the elastomer, as we said, the parameters of the mechanical model are assumed to be temperature dependent. They are determined from experimental measurements. These tests were realized for different temperature and followed by an interpolation law in order to obtain the evolution according to the temperature (Fig. 7).

5.2. Algorithm influence

The problem have to be solved on 14 s, so we consider two different configurations of the presented algorithm (see Fig. 4):

- First configuration: the natural configuration
 - $D_s = \phi_0$: mechanical source term,
 - $T_{\text{mec}} = T_{\text{the}} = 0.02$ s,
 - the thermal computation is realized considering the deformed geometry (i.e. computation of \overline{K}_L).
- Second configuration: the “simplified” configuration

According with Holzapfel and Simo [15] and Lion [22], the periodicity of the mechanical loading gives to the dissipation the same propriety (this phenomena is numerically verified on our model). So we choose a simplified configuration:

 - $D_s = \overline{\phi}_0(t) = \int_0^t \frac{\phi_0(s) ds}{t}$,
 - $T_{\text{mec}} = 0.93$ s (i.e. after three mechanical cycles, the dissipation is considered stabilized),
 - $T_{\text{the}} = 14$ s,
 - the thermal computation is realized on undeformed geometry.

The spatial discretization is given Fig. 9(b) and its characteristics Table 3. We verify on Fig. 8 that the two

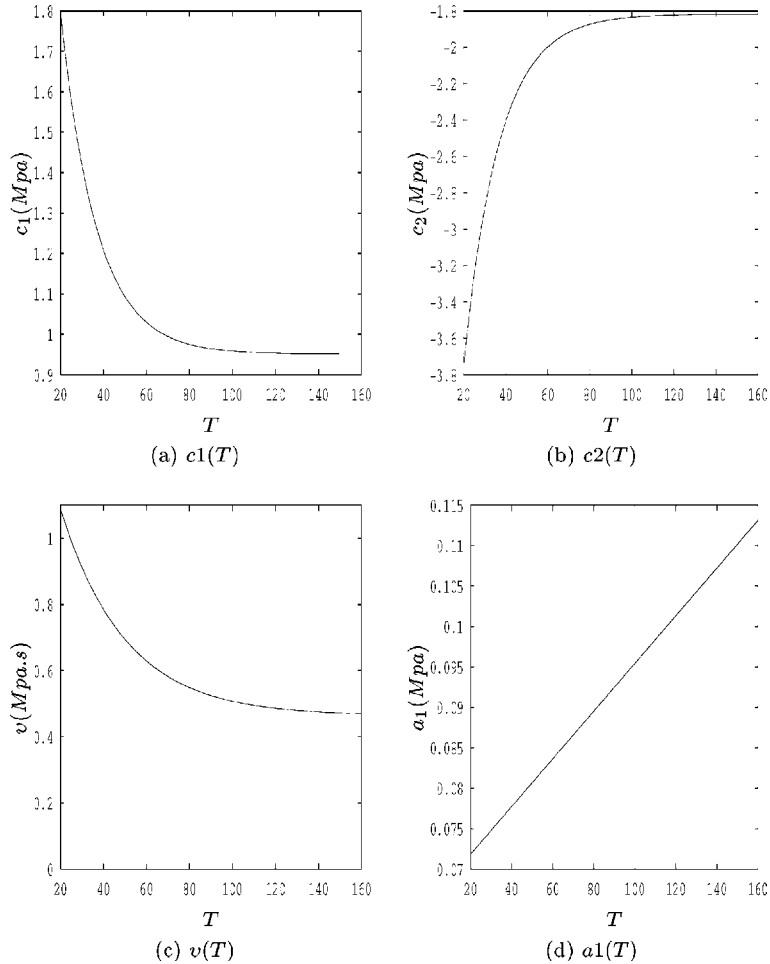


Fig. 7. Elastomer parameters according to the temperature.

Table 3

Numbers of elements and degrees of freedom according to the problem and the refinement

	Mechanical problem			Thermal problem	
	Elements	d.o.f. (displacement)	d.o.f. (pressure)	Elements	d.o.f. (temperature)
Refinement (a)	130	742	80	171	121
Refinements (b) and (d)	400	1938	320	459	285
Rrefinement (c)	1420	6250	1280	1515	853

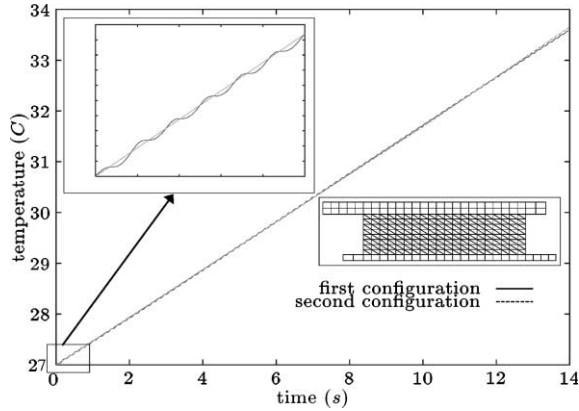


Fig. 8. Temperature evolution in the middle of the elastomeric layer. Comparison between the two configurations.

configurations algorithm give quite the same results. On the zoom, it is possible to see that the evolution obtained by the first repartition oscillate around the temperature obtained by the second one. More precisely, these oscillations have a period of two mechanical periods, be-

cause the dissipation is maximum when the mechanical loading is maximal or minimal. The first configuration need a CPU time fourteen time more important that the second one. For this reason, a generalization of the second configuration is adopted for the rest of the study, the i th cycle of it being:

$$\begin{cases} \text{mechanical computation } (\Delta t_{\text{mec}} = 0.888 \text{ s}) \\ + \text{thermal computation } (\Delta t_{\text{the}}^i = 2^{i-1} \times 10 \text{ s}). \end{cases}$$

5.3. Space discretization influence

5.3.1. Mesh refinement

Three spatial discretizations are declined (Fig. 9) and their characteristics are given in Table 3. In Fig. 10(a), we examine the maximum of the power balance obtained during the first mechanical computation, i.e. the quantity:

$$\rho_0 \dot{\psi} - \bar{\pi} : \dot{\bar{F}} - \phi^{\text{int}}. \quad (52)$$

Fig. 10(b) shows the maximum of the reactions reached during the the same mechanical time. At last, on Fig. 10(c), temperatures in the center (thermocouple 1,

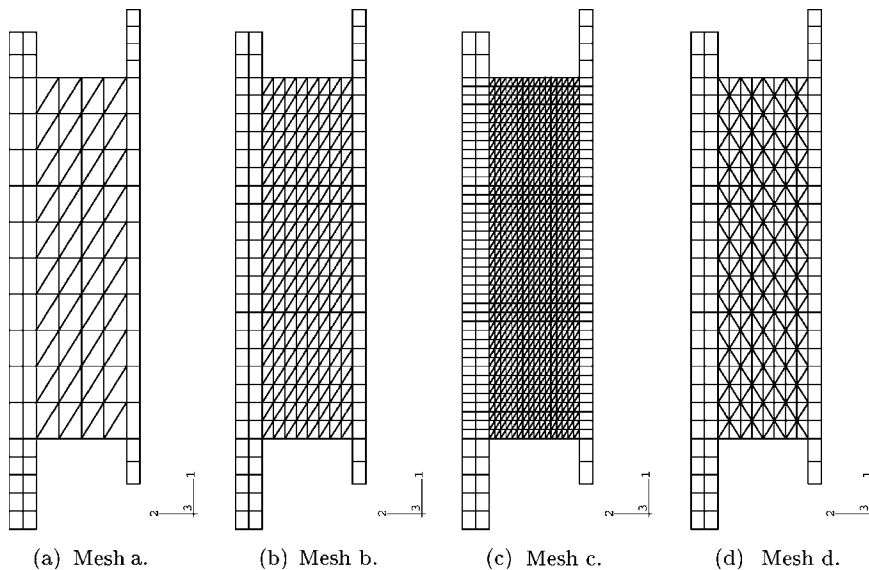


Fig. 9. Mesh refinement.

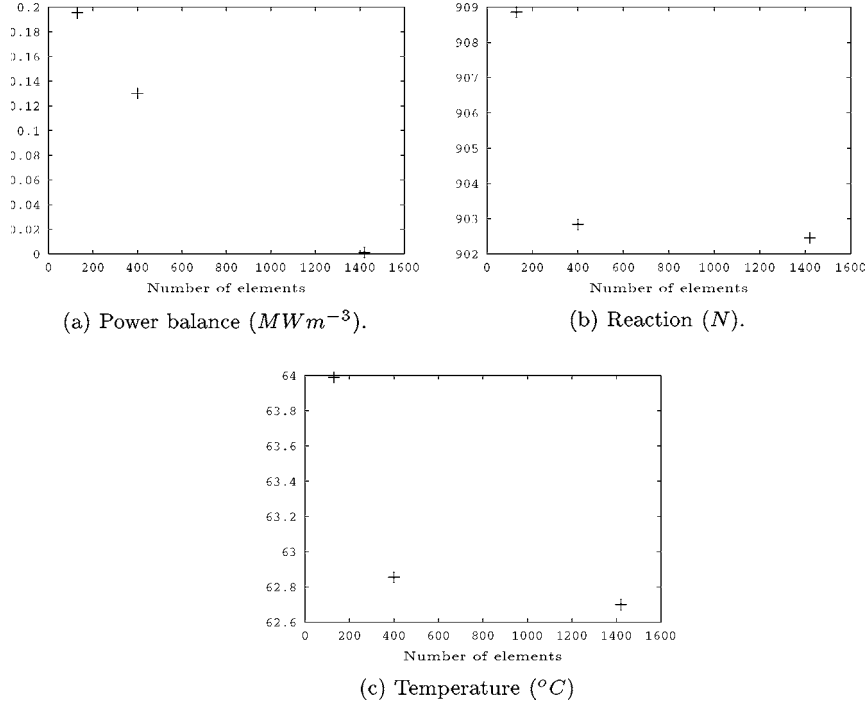


Fig. 10. Mesh refinement influence.

Fig. 6(a)) of the elastomeric layer are compared at the time 40 s for the three meshes.

All these investigations point that the more accurate mesh (c) gives the best results; but it also provides the more important CPU times. A good compromise between results validity and computational time, if the power balance is excluded, seems to be the mesh (b).

5.3.2. Type of mechanical spatial discretization

In this paragraph, the meshes (b) and (d) (Fig. 9(b) and (d)) are compared for a mechanical computation. These two discretizations present the same number d.o.f. (in displacement and pressure) and the same number of elements. We can see Fig. 11 that the mesh (d) is less conservative than the mesh (b).

5.4. Comparison with experiment

All the previous tests give a good idea of the space and times discretization to adopt.

From these results, two tests are realized, considering respectively a temperature of 25 and 60 $^{\circ}C$ for the thermal enclosure. The numerical results are compared on two positions (⊙, ⊗ see Fig. 12) with the experimental ones. This comparison gives a good agreement, and seems to validate the adopted discretizations (space and time) and at last the thermomechanical model.

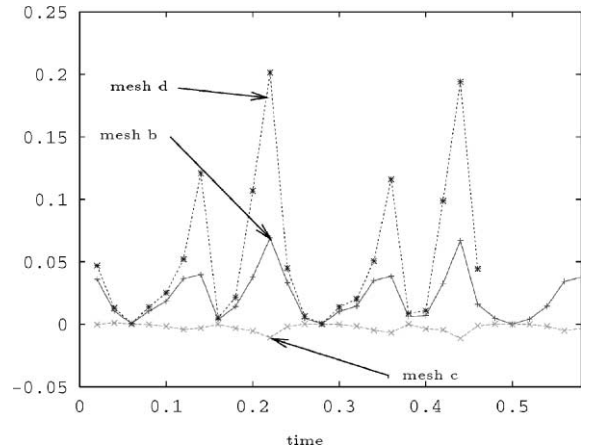


Fig. 11. Power balance over time ($MW m^{-3}$)—first mechanical cycle.

6. Conclusion

A new model has been developed to deal with mechanical and thermal problems, allowing for the interaction of both these phenomena. This explicit coupling has a solving algorithm adaptable to the two distinct time-scales. For the mechanical model, an hyperviscoelastic behavior is proposed. The thermal formulation is

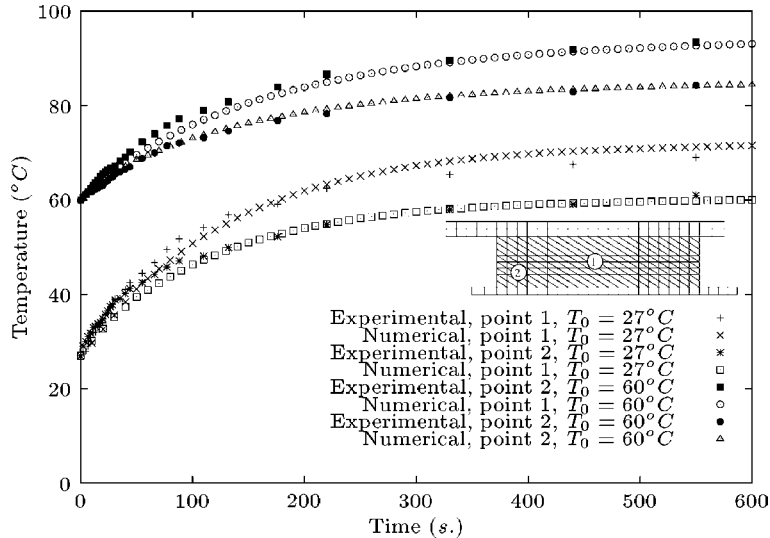


Fig. 12. Evolution of the temperature on two points of an elastomeric layer. Experimental and numerical results.

carried out under finite transformation hypothesis in the Lagrangian configuration in order to fit it to the mechanical formulation.

A study of space discretization allows to determine an appropriate refinement of mesh and a good pattern for it. We also obtain the increase of stiffness experimentally observed.

Finally, on a sinusoidal mechanical loading at two different initial temperatures, a comparison between numerical and experimental results gives some good results.

References

- [1] Bérardi G. Modélisation numérique du comportement thermo-viscoélastique dun élastomère en grandes déformations, 1995.
- [2] Carey GF, Oden JT. Finite elements. NJ: Prentice-Hall; 1986. vol. 2.
- [3] Chang WV, Bloch R, Tschoegl NW. The behaviour of rubber-like materials in moderately large deformations. *J Rheol* 1978;22:1–32.
- [4] Christensen RM. Theory of viscoelasticity, an introduction. New York: Academic Press Inc; 1971.
- [5] Coleman BD. Thermodynamics of materials with memory. *Arch Rational Mech Anal* 1964;17:1–46.
- [6] Coleman BD, Noll W. Foundations of linear viscoelasticity. *Rev Mod Phys* 1961;33:239–49.
- [7] Germain P, Mécanique 1 et 2. Cours de l'Ecole Polytechnique. Ellipses, 1986.
- [8] Glowinski R, Le Tallec P. Numerical solution of problems in incompressible finite elasticity by augmented Lagrangian methods, 2. Three-dimensional problems. *SIAM J Appl Math* 1984;44:710–33.
- [9] Govindjee S, Simo J. Transition from micro-mechanics to computationally efficient phenomenology: carbon black filled rubbers incorporating Mullins effect. *J Mech Phys Solids* 1992;40:213–33.
- [10] Govindjee S, Simo JC. A micro-mechanically based continuum damage model for carbon black-filled rubbers incorporating Mullins effect. *J Mech Phys Solids* 1991; 39:87–112.
- [11] Halphen B, Son NQ. Sur les matériaux standards généralisés. *J Méch* 1975;14:39–63.
- [12] Hart-Smith LJ. Elasticity parameters for finite deformations of rubber-like materials. *J Appl Math Phys* 1966;17: 608–26.
- [13] Harwood JAC, Mullins L, Payne AR. Stress softening in rubbers: a review. *J IRI* 1967:17–27.
- [15] Holzapfel GA, Simo J. Entropy elasticity of isotropic rubber-like solids at finite strains. *Comput Meth Appl Mech Eng* 1996;132:17–44.
- [16] Holzapfel GA, Simo J. A new viscoelastic constitutive model for continuous media at finite thermomechanical changes. *Int J Struct* 1996;33:3019–34.
- [17] Le Tallec P. Numerical analysis of viscoelastic problems. Paris: Masson; 1990.
- [18] Le Tallec P, Rahier C. Numerical models of steady rolling for non-linear viscoelastic structures in finite deformations. *Int J Numer Meth Eng* 1994;37:1159–86.
- [19] Lemaître J, Chaboche JL. Mécanique des matériaux solides. Paris: Dunod; 1996.
- [20] Leonov AI. On thermodynamics and stability of general Maxwell-like viscoelastic constitutive equations, theoretical and applied rheology. In: XIth International Congress on Rheology. 1992. p. 97–9.
- [21] Lianis G. Constitutive equations of viscoelastic solids under finite deformation. Purdue University Report, A&ES 63-11, 1963.
- [22] Lion A. On the large deformation behaviour of reinforced rubber at different temperatures. *J Mech Phys Solids* 1997;45:1805–34.
- [23] Malkus DS. Finite element with penalties in nonlinear elasticity. *Int J Numer Meth Eng* 1980;16:121–36.

- [24] Malkus DS, Hughes TJR. Mixed finite element methods—reduced and selective integration techniques: a unification of concepts. *Comput Meth Appl Mech Eng* 1978;15: 63–81.
- [25] Miehe C. Discontinuous and continuous damage evolution in Ogden-type large-strain elastic materials. *Eur J Mech, A/Solids* 1995;14:697–720.
- [26] Mooney M. A theory of large elastic deformation. *J Appl Phys* 1940;11:582–92.
- [27] Morman KN. Original contributions. an adaptation of finite linear viscoelasticity theory for rubber-like by use of the generalised strain measure. *Rheol Acta* 1988;27:3–14.
- [28] Mullins L. Effect of stretching on the properties of rubber. *J Rubber Res* 1947;16:275–89.
- [29] Oden JT. A theory of penalty methods for finite element approximations of highly nonlinear problems in continuum mechanics. *Comput Struct* 1978;8:445–9.
- [30] Oden JT, Kikuchi N. Finite element methods for constrained problems in elasticity. *Int J Numer Meth Eng* 1982;18:701–25.
- [31] Ogden RW. Large deformation isotropic elasticity, on the correlation of theory and experiment for incompressible rubber-like solids. *Proc Roy Soc, Lond A* 1972;326: 565–84.
- [32] Rivlin RS. Some topics in finite elasticity. In: 1st Symp on Naval Struct Mech, Stanford, August 11–14, 1958.
- [33] Sidoroff F. The geometrical concept of intermediate configuration and elastic finite strain. *Arch Mech* 1973;25(2): 299–309.
- [34] Sidoroff F. Un modèle viscoélastique nonlinéaire avec configuration intermédiaire. *J Méch* 1974;13(4):679–713.
- [35] Sidoroff F. Variables internes en viscoélasticité, 1. Variable internes scalaires et tensorielles. *J Méch* 1975;14(3):545–66.
- [36] Sidoroff F. Rhéologie non-linéaire et variables internes tensorielles. In: Symposium Franco-Polonais, Cracovie, 1977.
- [37] Simo JC. On a fully three-dimensional finite-strain viscoelastic damage model: formulation and computational aspects. *Comp Meth Appl Mech Eng* 1987;60:153–63.
- [38] Treloar LRG. The elasticity of a network of long chain molecules *i*. *Trans Faraday Soc* 1943;39:36–64.
- [39] Treloar LRG. The present status of the theory of large elastic deformations. In: *The Rheology of Elastomers*, 1957.